Journal of Applied Fluid Mechanics, Vol. 12, No. 6, pp. 2039-2055, 2019.
Available online at www.jafmonline.net, ISSN 1735-3572, EISSN 1735-3645.
DOI: 10.29252/jafm.12.06.29687

Theoretical, Numerical and Experimental Investigation of Secondary Injection with a Novel Pyrogenic Pulser

R. Taherinezhad† and G. Zarepour

Department of Mechanical Engineering, University of Guilan, Rasht, 51665-315, Iran

†Corresponding Author Email: shamsrtaher@phd.guilan.ac.ir

(Received October 4, 2018; accepted January 26, 2019)

ABSTRACT

In this paper, a novel pyrogenic pulser was designed both analytically and numerically and evaluated with empirical tests. The motivation of this study was the need for active control of the aero acoustic pressure oscillations by injecting the secondary flow into the solid rocket motor. First, in brief, pyrotechnic and pyrogenic pulsers have been introduced, and then analytical governing equations have been presented in three transient, sinusoidal and Hercules methods. In order to understand the internal pressure of the pulsar and its plume length, the injection flow field has been evaluated using the ANSYS-Fluent software with both $k-\omega$ SST and $k-\varepsilon$ Realizable models both at ambient and motor pressure. After that, the design and manufacturing of the pulser hardware and the test process have been described. Finally, analytical, numerical and experimental results have been discussed. The results show that there is a good correlation between the transient analysis in theory and the numerical solution by the k-ω SST model and the empirical test data. In addition, pyrogenic pulsers design depends on various parameters of motor and pulser charge performance prediction. The quality of pulser charge bonding to its insulator and erosion of its throat path due to injection have an important role to obtain a desirable pulser mass flow rate and plume length.

Keyword: Pyrogenic pulsers; Secondary injection; Solid rocket motors.

NOMENCLATURE

a	pressure coefficient
a_{ch}	speed of sound
A_{bi}	pulser burning surface
$\bar{C}_v$	mean constant volume specific heat
D_c	diameters of the motor chamber
D_v	diameter of pulser throat
F_n	volumetric and surface forces
F_{cn}	Control forces
h_c	pulser volume control source
k_n	wave number
L_p	pulser plume length
n	pressure exponent
p'	pressure oscillation
P_v	pressure of pulser throat
$\bar{P}$	mean chamber pressure
R	spatial distribution function
$\dot{r}$	burning rate
T	temperature
δP	pressure difference in motor
$\Re$	mean gas constant
$\eta_n(t)$	time-independent amplitude of the nth acoustic mode
ΔH_c	heat of combustion
$\psi_n(z)$	mode shape of the nth acoustic mode
ω_n	frequency
ρ	density
$\dot{m}_{inj}$	Secondary injection mass flow rate
ε	fraction of pulser mass flow to motor mas flow
$\dot{m}_{bi}$	mass flow rate outflows of pulser burning surface
γ	specific heat ratio
$\dot{m}_{ci}$	accumulation mass flow rate of pulser
β	constant of proportionality

Abbreviations

SST	Shear Stress Transport
ECP	Equivalent Chamber Pressure

1. INTRODUCTION

In the last seventy years, active control of aero acoustic pressure oscillations has been a serious challenge of designers in segmented large solid rocket motors (Zhang *et al.*, 2012), (Ferretti *et al.*, 2011). Literatures have referred to two methods for active control of pressure oscillations include of

acoustic excitation using a loudspeaker and secondary injection of a pulsating fluid (Poinsot *et al.*, 1989). The loudspeaker method is suitable only to instabilities with relatively small amplitudes and therefore not be useful for suppression of pressure oscillations in solid rocket motors (BILLOUD, *et al.*, 1992). It seems that secondary injection of a pulsating fluid is the best method for active control of aero acoustic pressure oscillations in solid rocket motors (Petersen & Murdock, 1999). Although secondary injection of both liquid and gaseous propellants has been used by other researchers (Bhattacharjee, 2013), but no injection of solid propellant has been used. Figure 1 indicates a scheme of motor chamber and a feedback controller with secondary fuel injection (Fung & Yang, 1992).The secondary fluid should be injected with a pulser at a sufficient mass flow rate to influence the motor pressure oscillation (Dehghani, 2014).

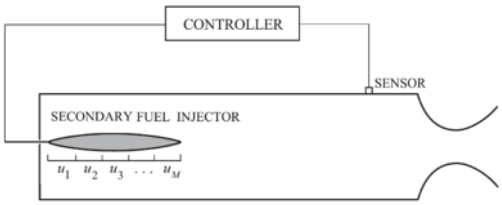

Fig. 1. Scheme of Active Control of Motor with Secondary Fuel Injection.

The pulsers can be divided into pyrotechnic and pyrogenic types, as shown in Fig. 2 (Baum & Levine, 1984). In pyrotechnic pulsers, shown in Fig. 2 (a), a charge of granular pyrotechnic propellant utilizing black or red gunpowder is ignited by an initiator and pulser pressure overstresses a diaphragm. Pulser gases vent into the motor chamber, creating a blowing gas flow (Golafshani & Loh, 1989). Figure 2 (b) indicates a pyrogenic pulser called "PSpyroi-1" has been used for a liquid rocket motor. The initiator of this pulser is positioned behind the end of the propellant grain and its output ignites the output end of this grain without igniting the internal surface of the grain or thermally damaging the grain structure (Hsiao & Saltus, 2006).

The concentration of this paper is on design and evaluation of pyrogenic pulser due to its efficient and reliable energy release and sustained combustion within the required time limit (Luke *et al.*, 1996), which provides the necessary mass flow rate to active control of aero acoustic pressure oscillations in motor. In fact, in the pyrotechnic pulsers, the explosion of a pyrotechnic fuel occurs, and therefore the discharge outlet from the pulser is released in a fraction of milliseconds, which is not suitable for blowing and controlling motor pressure fluctuations, but in pyrogenic pulsers, with more time, it can be used in active control by secondary injection. To determine the oscillatory flow field performance, pressure oscillation $p'(z,t)$ is defined as superposition of all harmonic with amplitude variables for each mode (Kreyszig *et al.*, 2011):

$$p'(z,t) = \bar{P}\sum_{n=1}^{\infty}\eta_n(t)\psi_n(z) \tag{1}$$

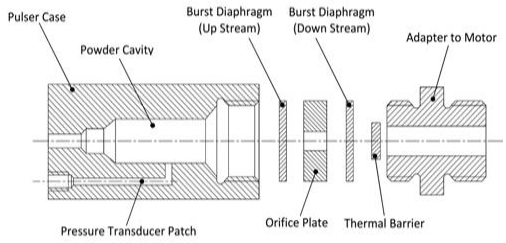

(a)

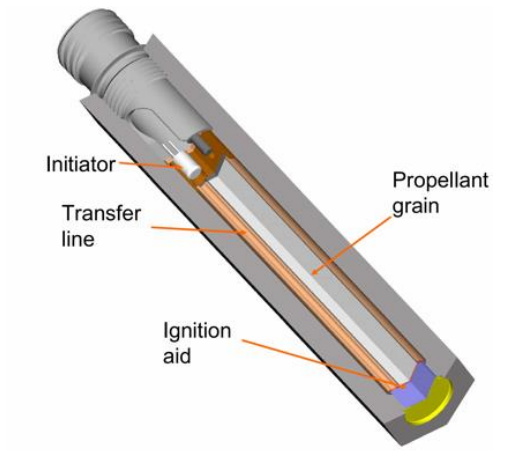

(b)

Fig. 2. Two kinds of Pulsers; a) Pyrotechnic, b) Pyrogenic.

where $\bar{P}$, $\eta_n(t)$ and $\psi_n(z)$ are mean chamber pressure , time-independent amplitude and mode shape of the nth acoustic mode, respectively. For closed chambers at both ends and purely longitudinal modes, $\psi_n(z)$ is (Blaett, 2011):

$$\psi_n(z) = \cos(k_n z) \tag{2}$$

and the value of $\eta_n(t)$ is calculated from the solution of second order differential equation as below (Bhattacharjee, 2013):

$$\ddot{\eta}_n + \omega_n^2\eta_n = F_n + F_{cn} \tag{3}$$

k_n, ω_n, F_n and F_{cn} are wave number , frequency ,volumetric and surface forces, exist in nature of motor burning control inputs, respectively. Secondary injection mass flow rate, $\dot{m}_{inj}$, displays itself in F_{cn}, can be wrote as (Culick & Kuentzmann, 2006):

$$F_{cn} = -\frac{\bar{a}^2}{\bar{P}E_n^2}\left\{\iiint h_c\ \psi_n dV + \oiint f_c\ \psi_n dS\right\} \tag{4}$$

When no surface control exists ($f_c = 0$), active control of aero acoustic pressure oscillation is done only with pulser volume control source h_c ,

demonstrating the effect of secondary injection mass flow rate (Yang *et al.*, 1992):

$$h_c(z,t) = -\frac{\Re \Delta H_c}{\bar{a}^2 \bar{C}_v}\left\{\ddot{m}_{inj}(t-\tau) R\left[z(\tau), t-\tau\right]\right\} \tag{5}$$

where $\Re$, $\bar{C}_v$, ΔH_c, $\dot{m}_{inj}(t)$ and $R[z(\tau),t]$ are the mean gas constant, the mean constant volume specific heat, the heat of combustion, the mass injection rate of the control fuel and the spatial distribution function characterizing the fraction of the fuel element burned at position z with a time delay τ, respectively. Therefore, determination of volume control source, h_c , needs to obtain of secondary injection mass flow rate, $\dot{m}_{inj}$, by a pulser.

2. GOVERNING EQUATIONS

Performance analysis of the pulserer is based on the solution of the continuity equation (Chen *et al.*, 2017). Since the pressure ratio across the throat is very high, it can be assumed to be choked. The pyrogenic pulser pressure should be substantially higher than the motor pressure, one would expect the pulser exhaust to be sonically choked and thereby the pulser pressure to decay exponentially (ADAMS, 1967). As shown in Fig. 3, mass flow rate $\dot{m}_{bi}$ outflows of pyrogenic pulser burning surface and with a few accumulation $\dot{m}_{ci}$, injects to motor chamber with $\dot{m}_{inj}$.

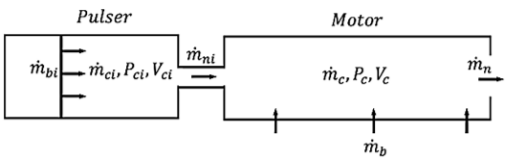

Fig. 3. Analytical Model for Secondary Injection in Motor.

2.1. Injection in Transient State

To understand the behavior of solid rocket motors, it is better to solve the internal ballistics under transient conditions (Greatrix, 2011). Assumptions for the pulser and motor performance are 1) mass flow rate accumulation is taken to account; 2) burning surfaces ignite uniformly; 3) pressure varies with time but temperature is constant; 4) burning rate follows the relation $\dot{r} = a(P)^n$ (Seifollahzadeh & Aminian, 2014); 5) isentropic, one-dimensional flow in exhausts; 6) ideal gases, $P/\rho = \Re T$ (Rousseau, 2011). From the continuity equation in the pulser (Sutton & Biblarz, 2010):

$$\dot{m}_{bi} = \dot{m}_{ci} + \dot{m}_{inj} \tag{6}$$

The first term in (6) can be written as (Zhang & Chou, 2006):

$$\dot{m}_{bi} = \rho_{pi} A_{bi} \dot{r}_{ci} = \rho_{pi} A_{bi} a_i P_{ci}^{\,n_i} \tag{7}$$

The third term for isentropic injection flow in pulser may be expressed by (Mossad & Deo, 2015):

$$\dot{m}_{inj} = \frac{A_{ti}\left(P_{ci} - P_c\right)}{c_i^*} \tag{8}$$

Finding the rate of $\dot{m}_{ci}$, it needs to differentiate density equation. In this case, variations of pressure are not negligible, due to it is also varying, but it can be safely neglected from variations of temperature and molecular mass (Humble *et al.*, 1995). The derivation of density relation gives:

$$\begin{aligned} m_{ci} = \rho_{gi} V_{fi} \Rightarrow dm_{ci} &= d\left(\rho_{gi} V_{fi}\right) \\ &= \rho_{gi} dV_{fi} + V_{fi} d\rho_{gi} \end{aligned} \tag{9}$$

where charge density ρ_{gi} and empty space volume of pulser V_{fi} are functions of time. On the other hand, empty space volume of pulser V_{fi} is equal to total space volume of pulser V_{ti} subtracting volume of pulser propellant V_{pi} . So time gradient of empty space volume of pulser will be equal to (Orieux *et al.*, 2002):

$$\begin{aligned} \frac{dV_{fi}}{dt} = \overset{0}{\frac{dV_{ti}}{dt}} - \frac{dV_{pi}}{dt} = -\frac{dV_{pi}}{dt} &= -A_{bi}\overset{-\dot{r}_{ci}}{\frac{dL_{pi}}{dt}} \\ &= A_{bi}\dot{r}_{ci} = A_{bi} a_i P_{ci}^{\,n_i} \end{aligned} \tag{10}$$

where L_{pi} is length of pulser propellant. Finally governing equation for transient state of pulser chamber can be obtained as:

$$\begin{aligned} \rho_{pi} A_{bi} a_i P_{ci}^{\,n_i} = \frac{A_{bi} a_i}{\Re T_{gi}} P_{ci}^{\,n_i+1} + \frac{V_{fi}}{\Re T_{gi}}\frac{dP_{ci}}{dt} \\ + \frac{A_{ti}}{c_i^*}\left(P_{ci} - P_c\right) \end{aligned} \tag{11}$$

and after simplification:

$$\frac{dP_{ci}}{dt} = c_1 P_{ci}^{\,n_i+1} + c_2 P_{ci}^{\,n_i} + c_3\left(P_{ci} - P_c\right) \tag{12}$$

where $c_1 = -\frac{A_{bi} a_i}{V_{fi}}$, $c_2 = \frac{\rho_{pi} A_{bi} a_i \Re T_{gi}}{V_{fi}}$ and $c_3 = -\frac{\Re T_{gi} A_{ti}}{V_{fi}\, c_i^*}$. Using the same method, the continuity equation in the motor can be wrote as:

$$\dot{m}_b + \dot{m}_{inj} = \dot{m}_c + \dot{m}_n \tag{13}$$

and so the final equation for motor pressure variations can be obtained:

$$\frac{dP_c}{dt} = c_4 P_c^{\,n+1} + c_5 P_c^{\,n} + c_6 P_c + c_7\left(P_{ci} - P_c\right) \tag{14}$$

where $c_4 = -\frac{A_b a}{V_f}$, $c_5 = \frac{\Re T_c \rho_p A_b a}{V_f}$, $c_6 = -\frac{\Re T_c A_t}{c^* V_f}$ and $c_6 = -\frac{\Re T_c A_t}{c^* V_f}$ Equations (12) and (14) are nonlinear ordinary differential equations that can be solved by numerical analysis using fourth-order Runge-Kutta method that yields smaller error terms (Polyanin & Manzhirov, 2007).

2.2. Sinusoidal Injection

The secondary injection can be assumed to be sinusoidal. For this purpose, the secondary mass flow

rate is given by (Petersen & Murdock, 1990):

$$\dot{m}_{inj} = \dot{m}_b \frac{\varepsilon}{2}(1+\sin\omega t) \tag{15}$$

where ε is $\dot{m}_{inj}/\dot{m}_b$, and ω is the injector frequency. After substituting Eq. (15) into Eq. (13) and integrating, the solution for motor pressure is given by:

$$\frac{P_c(t)}{P_o} = \left(1+\frac{\varepsilon}{2}\right) + \frac{\frac{\varepsilon}{2}B(B\sin\omega t - \omega\cos\omega t)}{B^2+\omega^2} + \frac{\varepsilon}{2}\left(\frac{\omega B}{B^2+\omega^2} - 1\right)\exp(-Bt) \tag{16}$$

where B is a constant depends on the total volume of the chamber, V, and the throat area, A_t, as follows:

$$B = \frac{A_t}{V_f}\sqrt{\gamma\Re T_c\left(\frac{2}{\gamma+1}\right)^{\frac{1}{\gamma-1}}} \tag{17}$$

Differentiating the second term in Eq. (16) and setting it equal to zero, the maximum pressure perturbation due to secondary injection will be obtained:

$$\frac{P'_{P-P}}{P_o} = \frac{\varepsilon B\left\{B\sin\left[\tan^{-1}(-B/\omega)\right] - \omega\cos\left[\tan^{-1}(-B/\omega)\right]\right\}}{B^2+\omega^2} \tag{18}$$

2.3. Hercules- Aerojet Analysis

Hercules and Aerojet companies have analyzed pyrotechnic pulsers. In Hercules analysis, the pulser chamber immediately aft of the rupture diaphragm/orifice assembly is treated as a classical shock tube, which forms at the orifice plate, travels through the motor mounting adapter (Fig. 4), and expands in a quasi-spherical manner into the test chamber (Blomshield *et al.*, 1997). In Fig. 4 , D_v and P_v are the diameter and pressure of pulser throat, respectively and δP is pressure difference in motor due to pulsation. The relationship between the throat pressure,P_v, and internal pressure of the pulser, P_{ci}, is defined by pressure relation in isentropic flow with choked throat as (Olaoye & Abdulhafeez, 2012):

$$P_v = \left(\frac{\gamma+1}{2}\right)^{-\frac{\gamma}{\gamma-1}} P_{ci} \tag{19}$$

Based on Hercules analysis, pressure difference δP is defined as (Blomshield *et al.*, 1997):

$$\delta P = (P_v - P_c) \Big/ \sqrt{1+1.75\left(\frac{D_c}{D_v}\right)^2} \tag{20}$$

where D_c and D_v are the diameters of the motor chamber and connecting tube.

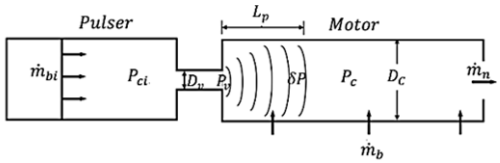

Fig. 4. Simplified Schematic of Hercules- Aerojet Pulser Test Setup.

In Aerojet developed analysis (Blomshield *et al.*, 1997), mass and energy balance equations are applied to the combustion chamber. These take the form of two ordinary differential equations with pressure and temperature as dependent variables, and when solved simultaneously, yield the amplitude of the pulse introduced into the test chamber. The pulse amplitude,δP, is related to the mass of pulser gases injected into the test chamber, $\dot{m}_{inj}$:

$$\delta P = \frac{t_c \beta a_{ci}^2 \dot{m}_{inj}}{g\gamma_{ci} A_c L_p} \tag{21}$$

where $\beta = D_c/D_v$, a_{ch} ,γ_{ch}, A_c ,L_p and t_c are a constant of proportionality, speed of sound, specific heat in the pulser, motor port area, pulser plume length and the time period of the motor first longitudinal mode, respectively. Using Eqs. (19) to (21), secondary injection mass flow rate can be obtained as:

$$\dot{m}_{inj} = \frac{g\gamma_{ci}A_c L_p}{t_c \beta a_{ci}^2}\left[\left(\frac{\gamma+1}{2}\right)^{-\frac{\gamma}{\gamma-1}} P_{ci} - P_c\right] \Big/ \sqrt{1+1.75\left(\frac{D_c}{D_v}\right)^2} \tag{22}$$

In pulser design, it should be attended that pulser and motor pressures influence on each other. Pulser pressure should be greater than motor pressure to outflow pulsation products to motor. Also, because of active control requirements, pulser pressure should be responder to pulser mass flow rate $\dot{m}_{inj}$ and plume length L_p.

2.4. Results of Governing Equations Solution

Table 1 demonstrates input values of transient analysis of Pulser and motor Internal Ballistic. In this study, active control design needs to have a minimum pulser plume length of $L_p = 570\,mm$ in motor. To this end, pulser plume in ambient should be a minimum length of $L_p = 168\,mm$. In real, measurement of pulser plume length in motor is impossible and so authors decided to test and record pulser injection in ambient and then compare the plume length pictures with ambient length of pulser plume calculation, both in analysis and Ansys-Fluent. It seems that, if pulser length from ambient test is accordance with theoretical calculations, then it is acceptable that pulser length in motor will be the same of theory.

Figures 5 to Fig. 7 represent pulser and motor performance prediction in various injection analysis types during motor action times 0-1 and 1.5-2.5 s. This time division has been decided due to motor pressure variations versus time.

Table 1 Input Values of Transient Analysis of Pulser and Motor Internal Ballistic

Item	Symbol	Unit	Pulser Value	Motor Value
Pressure Coefficient	a	m/s	7.04	1.601
Pressure Exponent	n	m	0.31	0.435
Temperature	T	ºK	3200	3200
Gas Constant	R	J/kg. ºK	320	320
Characteristic Velocity	c^*	m/s	1550	1550
Propellant Density	ρ	kg/m^3	1758	1758
Initial Pressure	P_o	bar	0.82	0.82
Throat Dia.	d_t	mm	3	45
Initial Burning Surface	A_{b_i}	mm^2	415.476	287544.19
Empty Distance	L_e	mm	4	-
Initial Empty Volume	V_i	mm^3	1661.9	2483902.48
Time Step	h	s	0.001	0.001
Plume Length in Ambient	L_p	mm	168	570

Figure 5 demonstrates that when pulser injects in ambient, its pressure is about 30 bar, but when injecting in motor with pressure about 40 bar, its pressure is higher than 40 bar and differs between 50 to 60 bar for transient analysis and 40 to 60 bar for sinusoidal injection type. On the other hand, transient pressure trace of pulser is the same as motor with a positive shift, but sinusoidal pressure trace differs.

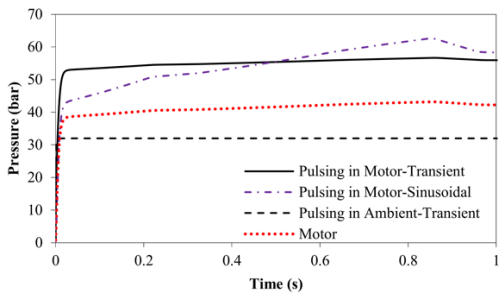

a) t=0-1 s

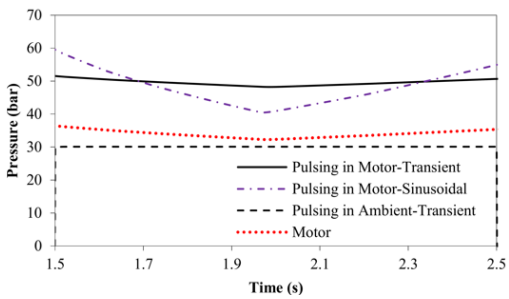

b) t=1.5-2.5 s

Fig. 5. Pulser Pressure Prediction.

Figure 6 demonstrates that transient pulsing produces maximum gage pressure difference in motor relative to other methods. Figure 7 demonstrates that when pulser injects in ambient, its mass flow rate is about 0.015 Kg/s, but when injecting in motor, its mass flow differs between 0.015 to 0.03 Kg/s and its average is for transient analysis with the value of 0.02 Kg/s.

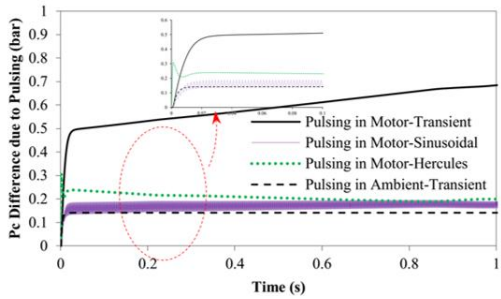

a) t=0-1 s

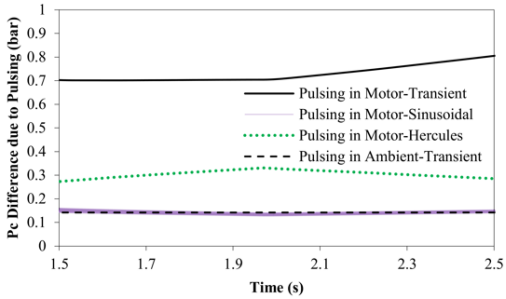

b) t=1.5-2.5 s

Fig. 6. Motor Pressure Shift Prediction due to Pulser Injection.

3. Numerical Solution of Pulser Flow Field

To help in understand the behavior of pulsation fluid, 2D flow has been solved using the computational fluid dynamics software "ANSYS-FLUENT", due to its good capability and user friendliness (Kostić *et al.*, 2015). Two turbulent models, the $k-\varepsilon$ realizable and the shear stress transport $k-\omega$ SST, were used in this work to examine which one predicts the flow more closely to the measured values (Zhao *et al.*, 20181). Solver was taken as density based and

formulation as implicit, space as 2D and time as steady (Dehghani, 2014). Solution initialization was done at first with Hybrid method and then Full-Multi-Grid (FGM) was used (*Satyanarayana et al.*, 2013). For CFD analysis of the present wok, combustion was not considered (Anthoine *et al.*, 2000). The flow was assumed to be incompressible, hot, 2D axisymmetric, viscous flow, ideal gas and uniform injection of fluid normal to boundary (Roach *et al.*, 1992). Under-Relaxation Factors include of turbulence kinetic energy, dissipation rate, viscosity and courant number, were set as 0.8, 0.8, 1 and 10, respectively. Discretization Equation includes of gradient, flow, turbulence kinetic energy and dissipations rate, were selected as least square cell based and second order up wind, respectively. The properties of gas include of specific heat, thermal conductivity, viscosity and molecular weight were taken as 1901 J/Kg.ºK, 0.034 W/m.ºK , 9×10^{-5} Kg/m.s and 28.23 Kg/Kmol, respectively.

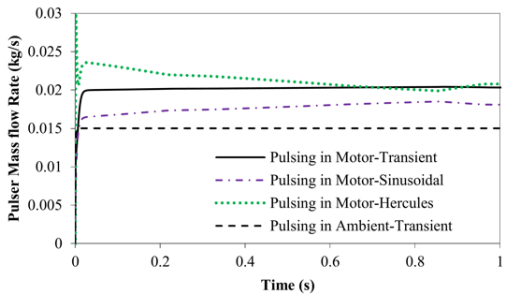

a) t=0-1 s

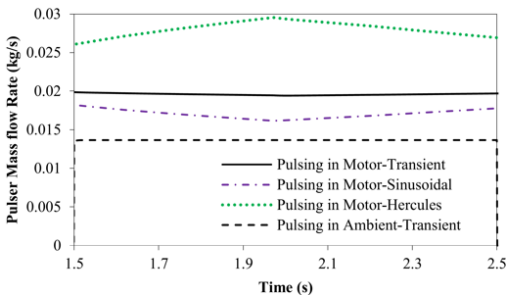

b) t=1.5-2.5 s

Fig. 7. Pulser Mass Flow Rate Prediction.

3.1. Pulser Injection in Ambient

Figure 8 represents the segmentation of pulsation flow field and mesh with 64000 quadrilateral grids. Meshing field is divided to three sections 1, 2 and 3 that are from pulser burning surface to the end of pulser throat, from pulser exhaust to end of conical part and developed region of plume, respectively. Note that origin of coordinate system is on pulser exhaust. Evaluation of grid resolution was done to obtain acceptable results in CFD including of 21000, 41000 and 64000 grids. As shown in Fig. 9, difference of Mach number results between 21000 and 41000 grids is obvious with the maximum error of 93%, but when grid became finer to 64000 grids, this difference, nearly, eliminated with the maximum error of 8.9%. Similar behavior was observed in other results like pressure and velocity. As shown, y^+ values from pulser throat beginning to pulser exhaust are in the range of 40 to 60. Because of using turbulent models $k-\varepsilon$ Realizable and $k-\omega$ SST, there is no need to very small meshing (y^+<4) near the pulser throat wall due to using of Wall Function for velocity gradient calculation (Dehghani, 2014).

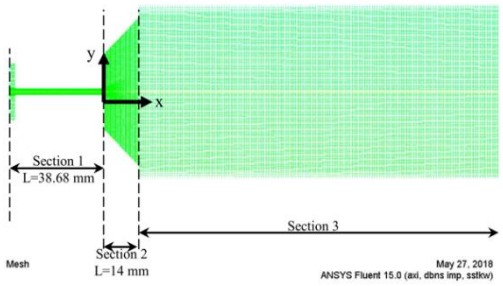

Fig. 8. Pulsation Flow Field and it's Meshing.

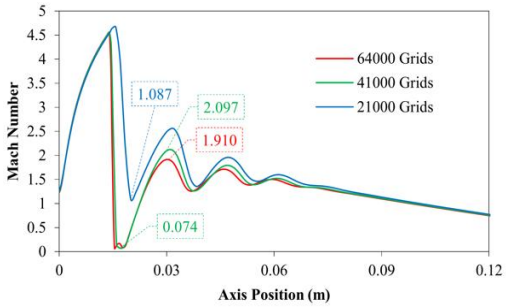

Fig. 9. Evaluation of Grid Resolution on CFD Results.

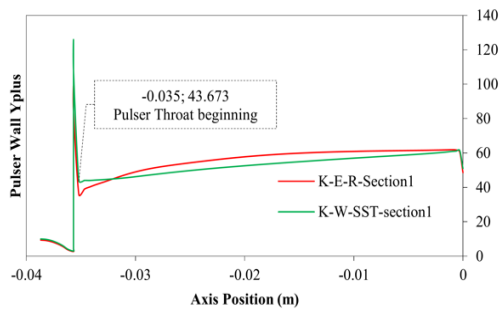

Fig. 10. Evaluation of y^+ Results on Pulser Throat Wall.

Boundary condition has been taken as mass flow inlet equal to 0.014 Kg/s from pulser burning surface, temperature as 3200 ºK in pulser, initial gauge pressure as 0.82 bar and ambient temperature as 3200 ºK. Figs. 11 to 13 represent Mach, temperature and velocity contours of pulser injection in ambient with two models of $k-\varepsilon$ Realizable and $k-\omega$ SST. In all figures, effective length of contours has been specified. As shown, contours length of $k-\omega$ SST model is higher and more developed than $k-\varepsilon$ Realizable model. So, it seems that in numerical approach done with ANSYS-Fluent, $k-\omega$ SST turbulent model gives a better answer than $k-\varepsilon$ Realizable model. In the future sections, this opinion will be confirmed in comparison with test results.

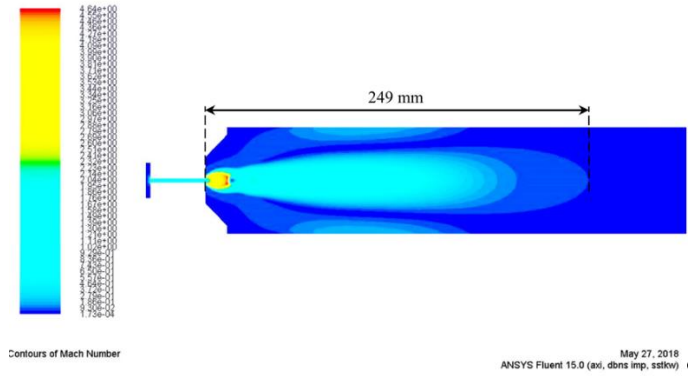

a) $\boldsymbol{k-\omega}$ SST

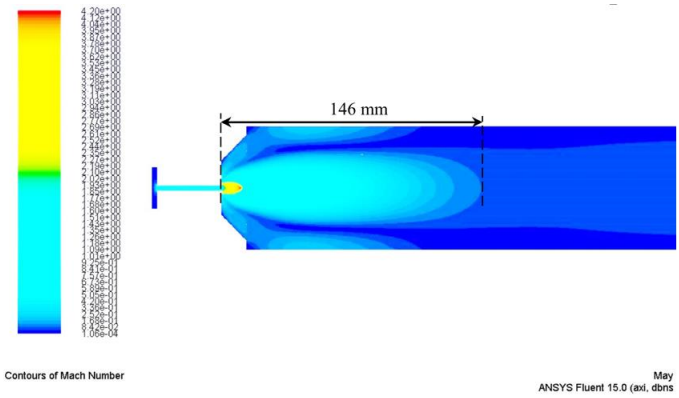

b) $\boldsymbol{k-\varepsilon}$ Realizable

Fig. 11. Mach Contour of Pulsation in Ambient.

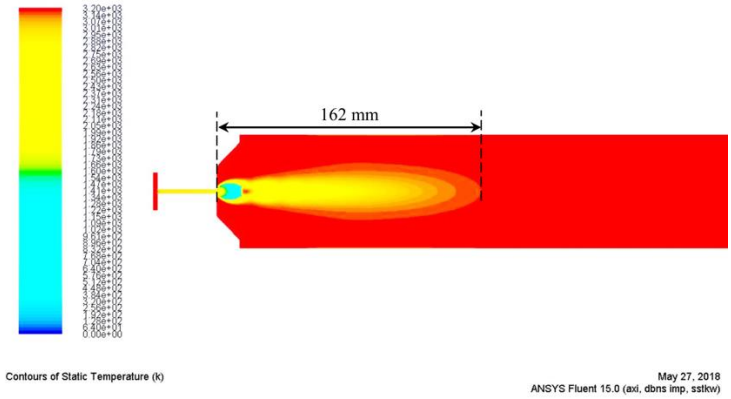

a) $\boldsymbol{k-\omega}$ SST

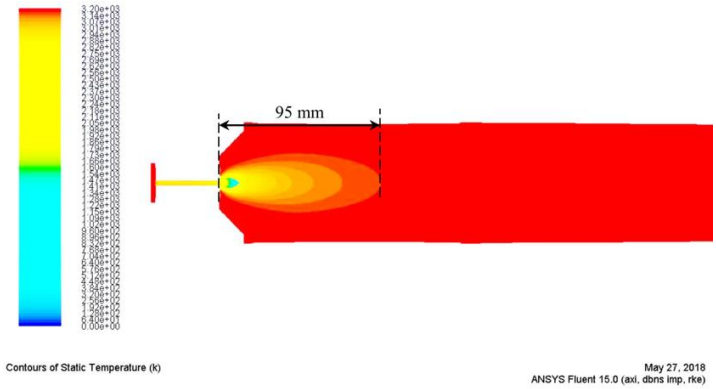

b) $\boldsymbol{k-\varepsilon}$ Realizable

Fig. 12. Temperature Contour of Pulsation in Ambient.

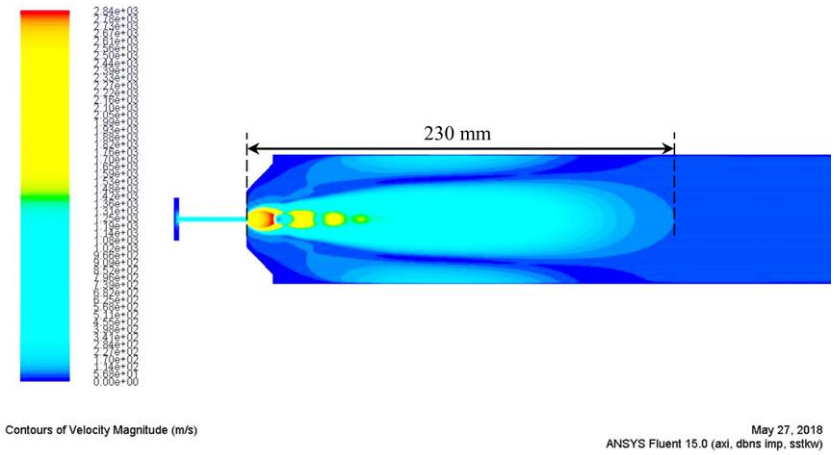

a) $\boldsymbol{k-\omega}$ SST

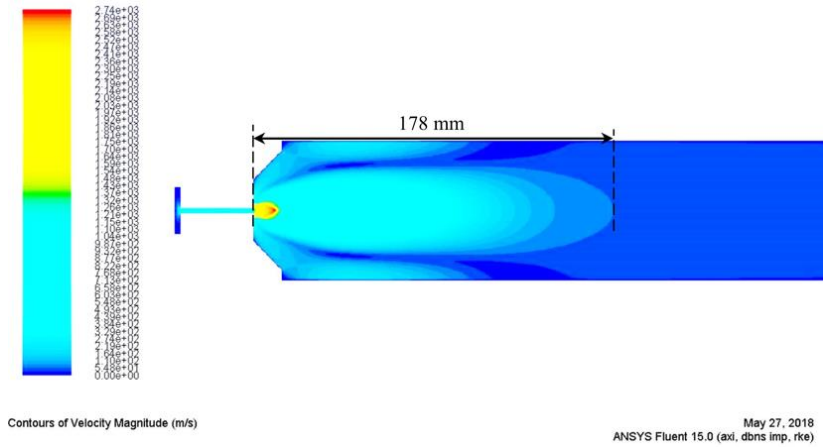

b) $\boldsymbol{k-\varepsilon}$ Realizable

Fig. 13. Velocity Contour of Pulsation in Ambient.

Figure 14 CFD Mach Number Results on Pulser and Motor Axis due to Pulsation in Ambient.represents Mach number and static absolute pressure variations through pulser and motor axis due to pulsation in ambient. As shown, Mach number in pulser throat reaches to one, increases to 4.5 in pulser exhaust, decreases to 0.067 at x=0.214 m and finally become constant.

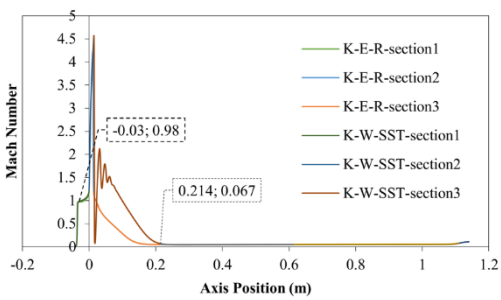

Fig. 14. CFD Mach Number Results on Pulser and Motor Axis due to Pulsation in Ambient.

As shown in Fig. 15, pressure decreases from about 37 bar on pulser burning surface to about 21 bar in pulser throat inlet and then to 15 bar in pulser exhaust. It is interesting that similar to Mach number, static pressure in pulser plume decreases to 0.836 bar in x= 0.214 m and finally become constant. Really, it seems that effective plume length is up to x=0.214 m and thereafter ebbed.

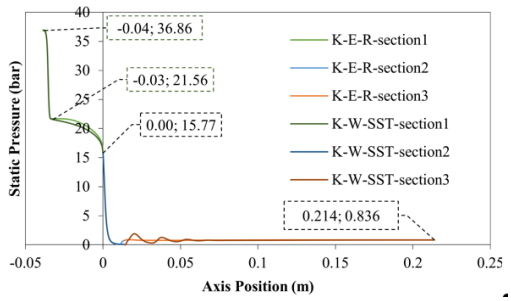

Fig. 15. CFD Static Pressure Results on Pulser and Motor Axis due to pulsation in Ambient.

3.2. Pulser Injection in Motor

The solid rocket motor used in this research, is 1:30 sub scale of shuttle boosters whereas geometrically, kinematically and dynamically are similar together (Doisneau *et al.*, 2012), using Buckingham's theorem (Richard *et al.*, 2012). Figure 16 shows 3D

modeling and manufactured scheme for subscale motor with outside diameter 122 mm, length 1270 mm and throat diameter 45 mm. The case is made of 4130 steel with welded flanges and connection of segments is M6×30 bolts. For simplicity of manufacturing and time frugality, throat has been made of Ta-Cu material.

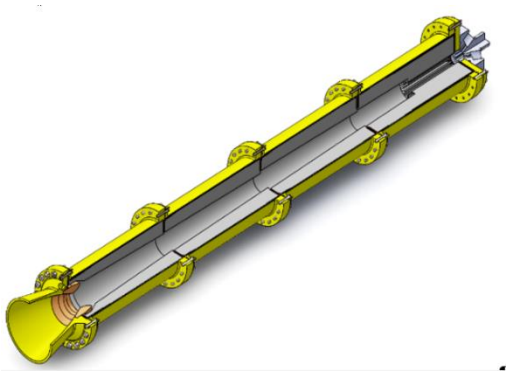

Fig. 15. 3D Model of Sub scaled RSRM.

Shape of the thermal inhibitor between segments of propellant can be taken either rigid (Vuillot, 1995) or flexible (Richard *et al.*, 2012). In this project, it is assumed rigid with considering ablation in definite modeling time. Estimated values of the wall Y^+ value for this grid shows it to be less than 30 along the entire wall, indicating good resolution of the boundary layer (Abdul Raheem & Babu, 2004). To simulate pulsation flow in motor, exhaust flow from pulser and motor burning surfaces has been solved in steady state with pulser mass flow rate of 0.021 Kg/s. Figure 17 represents the temperature and velocity contours due to pulsation in motor. As shown, there is not a distinct boundary between them due to pulser and motor flows combination. Although the flow core length, in Fig. 17(b), is to x=142-285 mm, but it seems that the effects of pulser injection on motor internal flow reaches to position x=570 mm.

Figs. 18 to 20 represent comparison between motor velocity contour, Mach number and static absolute pressure with and without pulsation through motor axis, respectively. As shown in Fig. 18, pulser injection changes the standing velocity contours in motor to conical at least to x=0.57.

According to Fig. 19, Mach number starts with zero value on pulser burning surface and increases to one in pulser throat. Also Mach number with pulsation is a few higher than without pulsation and this difference becomes lower through motor axis and zero in position x=0.85 m.

Figure 20 shows that pressure value on pulser burning surface is about 62 bar and decreases to 44 bar in pulser throat. Detailed view, also, shows that pressure trace has a similar behavior of Mach number.

Figure 21 compares static pressure results of CFD between pulsation in motor and ambient. As shown, pressure difference in pulser chamber is about 25 bar with a similar behavior. After outflowing from pulser exhaust, although pressure trace of pulsation in motor follows the motor pressure, but in ambient, plume pressure decreases to ambient pressure about 0.82 bar.

4. Pulser Test

As obtained from the analytical calculations, to achieve the requirement of one second injection with a mass flow rate of 0.015 Kg/s at 40 bar and 0.02 Kg/s at 60 bar for pulsation in ambient and motor, respectively, pulser charges were made from pyrogenic solid propellant with the burning rate of 30 mm/s at mean pressure of 90 bar, obtained from strand burner, diameter of 23 mm and length of 30 mm. Necessity of end burning design leads to produce pulser propellant in PTFE tubes, as shown in Fig. 22(a), to protects charge from side burning. After producing pyrogenic charge, it is placed in a steel case with a thread connection, as shown in Fig. 22 (b).

All charged pulsers and motor igniter installed on a steel connector, shown in Fig. 23(a). The reason for such a design was the limitation in the dimensions of the motor and the need for installing the pulsers and igniter on the motor head end. The initiator used for any of the pulsers and the igniter, is a simple glow plug with two high-resistance bridge wires buried in the initiator charge (Humble *et al.*, 1995), installed in a minimum distance to burning surfaces of pulser and igniter, shown in Fig. 23 (b). When initiator fires, combustion products outflow of pulser path, stroke a closure and discharge to ambient or motor. The closure bonded to connector case with RTV and its role is to protect pulser pyrogenic charge from motor flame and undesirable ignition.

4.1. Pulser Injection Test in Ambient

In the first test, one pyrogenic pulser fired in ambient with delay time of 51 ms. Figure 24 and Fig. 25 represent temporal pictures of pulsation plume that has been taken with a high speed camera and the pulser chamber pressure-time curve, respectively. As shown, pulser burning has a good behavior until t=225 ms with a desired pressure of 30-35 bar. But thereafter, the pressure increases suddenly up to 157 bar and then decreases.

For evaluation of pulser plume behavior and its pressure variations, the second test fired in an equivalent chamber. As shown in Fig. 26, equivalent chamber is an opened end tube with the length and diameter of free volume of motor grain which pulser connector installed on its head end and four Celltec pressure transduces installed on external side of tube.

Figure 27 to Fig. 29 represent temporal pictures of pulsation plume, pulser chamber pressure and ECP, respectively. As shown in Fig. 27, pulser outflow of equivalent chamber is nearly normal until t=637 ms and thereafter, clearly, enlarged in t=645 ms.

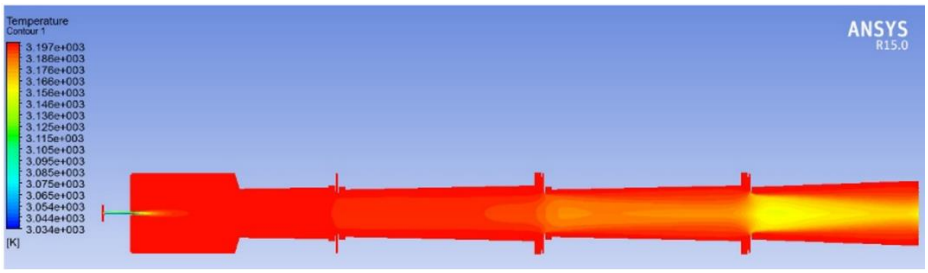

(a)

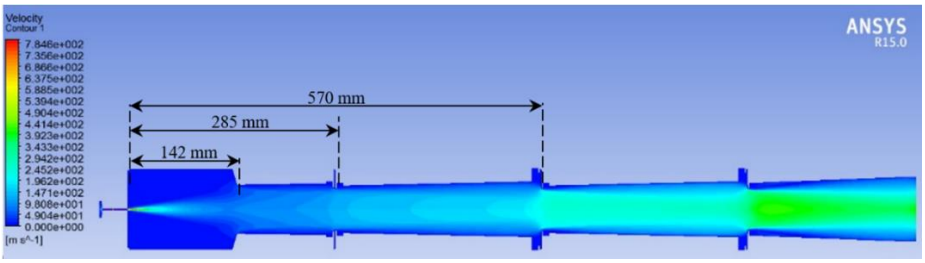

(b)

Fig. 16. Results of Pulsation Flow Filed Solution in Motor; a) Temperature and b) Velocity.

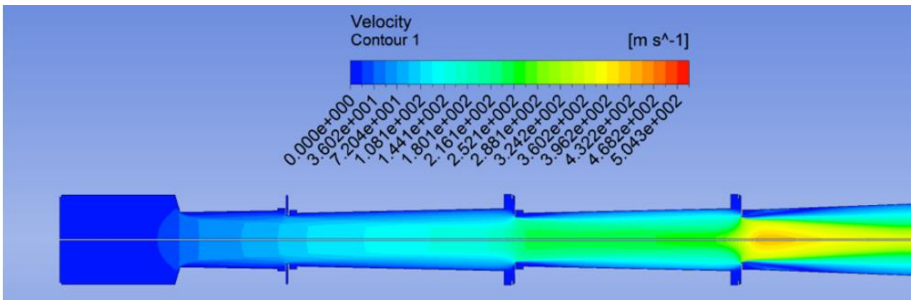

(a)

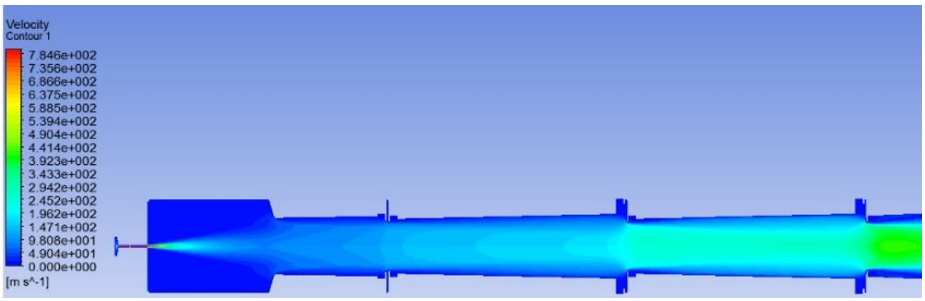

(b)

Fig. 17. Comparison between Motor Velocity Contour; a) with and b) without Pulsation.

Figure 28 shows that second test has a stable burning time to t=645 ms which is more than the first test. However, thereafter, the pressure increases suddenly up to 400 bar and then decreases. Data acquisition from pressure transducers on tube has shown in Fig. 29. Note that these are gage pressures relative to ambient pressure of 0.82 bar.

As shown in Fig. 29(a), plume pressure level in P1 is closer to prediction and higher than other positions. On the other hand, pressure level in P2 and P3 is nearly similar but in P4 is lower than others. These differences have been shown in detailed view of Fig. 29(b). Sinusoidal behavior of pulme pressures is due to reciprocating waves in the Equivalent Chamber tube.

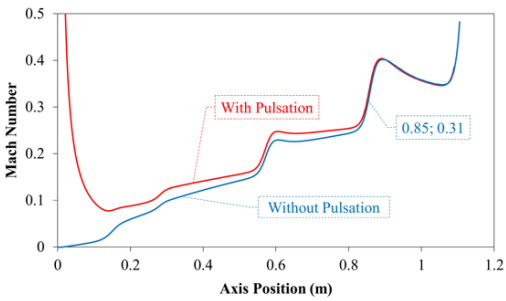

Fig. 18. Mach number on Comparison Motor Axis with and without Pulsation.

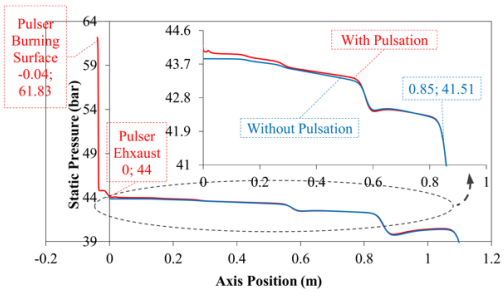

Fig. 19. Static Pressure Comparison on Motor Axis with and without Pulsation.

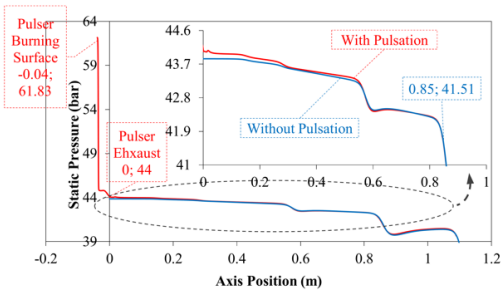

Fig. 20. Static Pressure Comparison on Motor Axis with and without Pulsation.

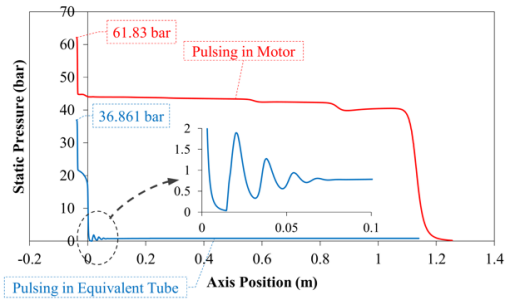

Fig. 21. Static Pressure Comparison between pulsation in motor and ambient.

(a)

(b)

Fig. 22. Pulser; a) Pyrogenic Charges, b) Filled Case.

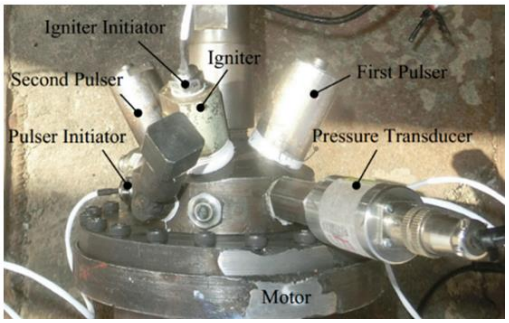

a) Assembled

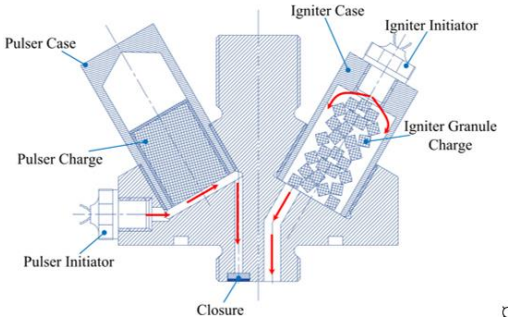

b) Cross Sectional Scheme

Fig. 23. Pulser Connector.

4.2. Pulser Injection Test in Motor

As shown in Fig. 23 (a), two pulsers were chosen to pulsate in motor. Figure 30 represents simultaneous demonstration of pressure data acquisition from motor and two pulsers where fired at t=0.25 s and t=1.7 s, respectively. Using bisector rule (Sutton & Biblarz, 2010), burning rate of the first pulser is obtained as t_b=1.22 s and the second as t_b=1.27 s. Clearly, pulser pressure pattern due to pulsation in motor is similar to motor pressure curve with a positive shift, as referred in analytical calculation and since pulsation is finished, internal pressure of each pulser is matched with motor pressure. Pressure difference between two pulsers and motor pressure, as shown in Fig. 31, is about 8.9-12.7 and 6.2-8 bar with average of 10.8 and 7.1 bar, respectively.

5. DISCUSSION

In Eq. (13), it is clear that the discharge from the pulser is directly related to the motor burning discharge, the accumulation flow, and the discharge of the motor. On the other hand, the pulser and the motor mass flow are dependent on the internal pressure of each one, and therefore, mass flow will definitely affect the motor's pressure. This description was added to the article text.

As shown in Table 2, a variation of pulser behavior was observed due to initiator performance, pulser charge burning sensitivity, delay time, sudden enhancement of pulser burning surface and throat diameter, and differences between pressure coefficients a and n, obtained from strand burner laboratory test and real static test.

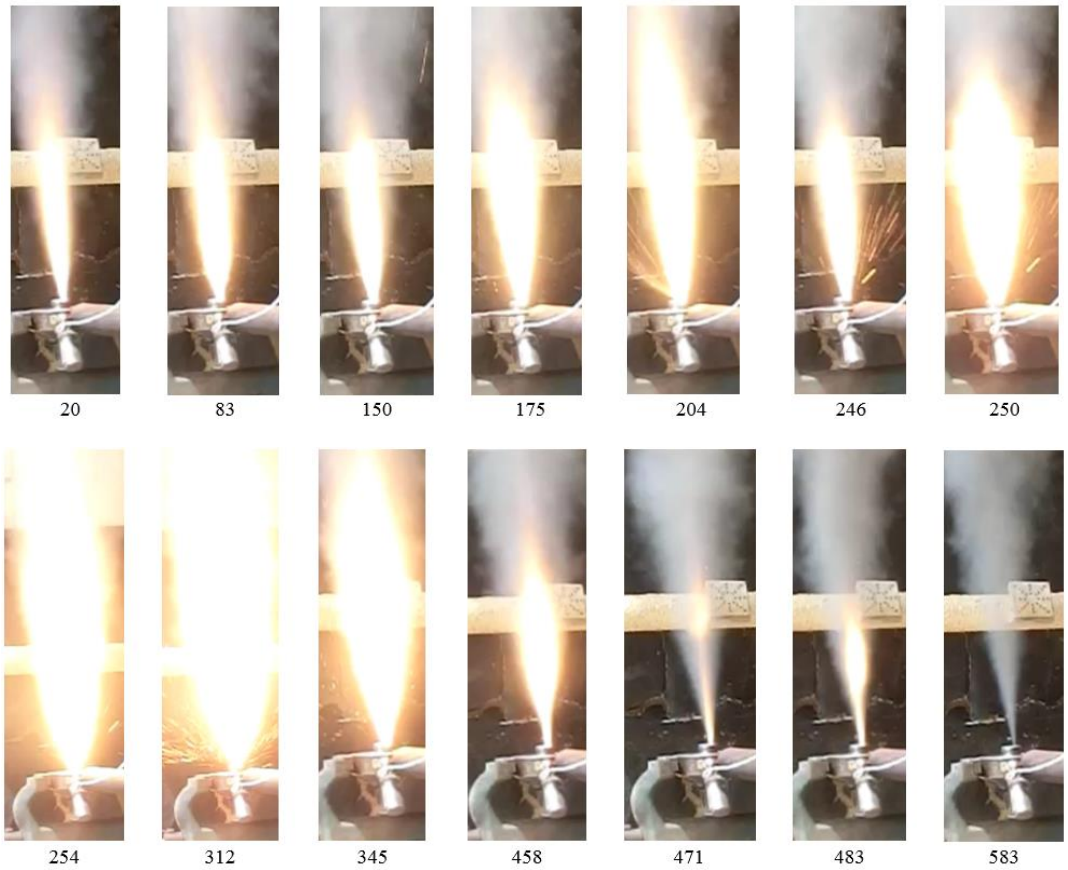

Fig. 24. Temporal Pictures of pulsation in ambient in millisecond.

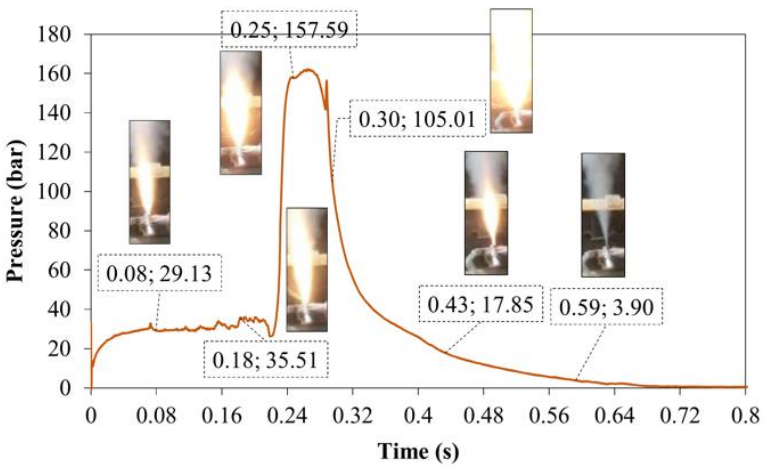

Fig. 25. Pulser Pressure due to Pulsation in Ambient.

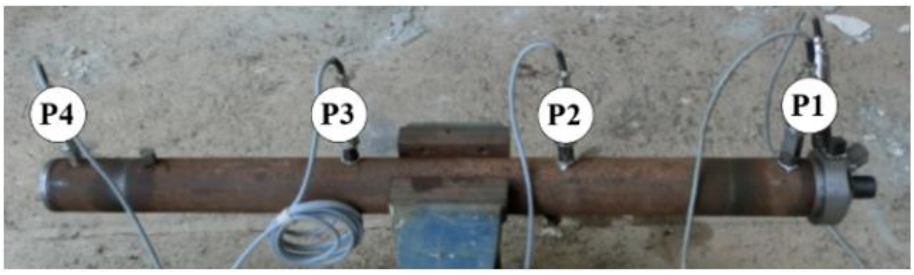

Fig. 26. Equivalent Test Chamber for Identification of Pulser Plume in Ambient.

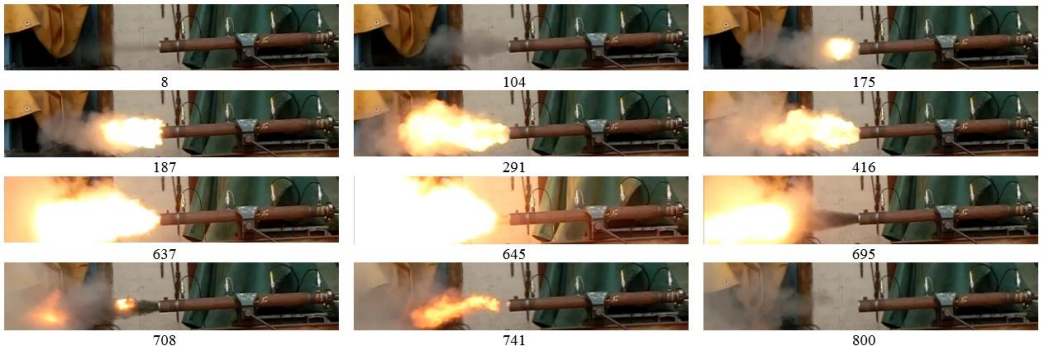

Fig. 27. Temporal Pictures of pulsation in Equivalent Test Chamber in millisecond

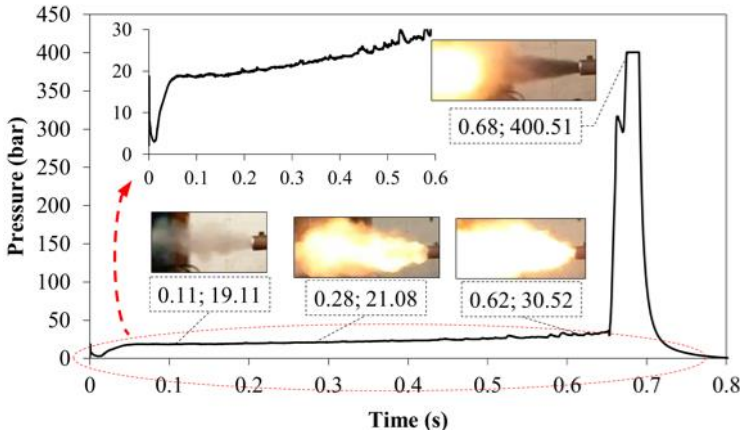

Fig. 28. Pulser Pressure due to Pulsation in Equivalent Chamber.

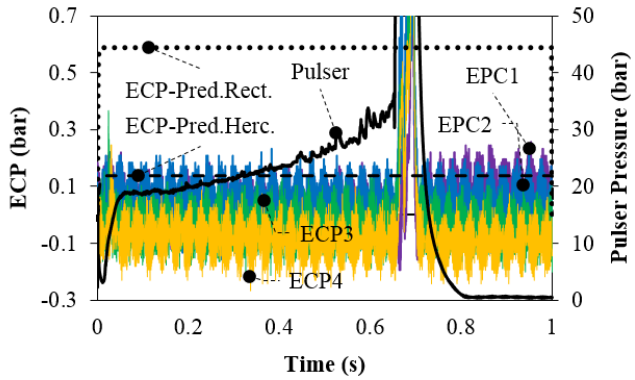

(a)

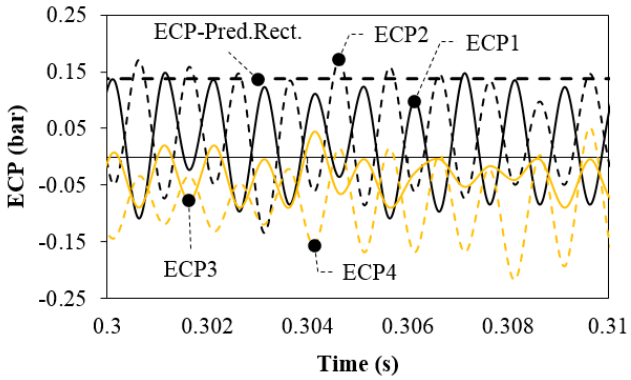

(b)

Fig. 29. ECP due to Pulser Plume; a) Overall b) Detailed Time.

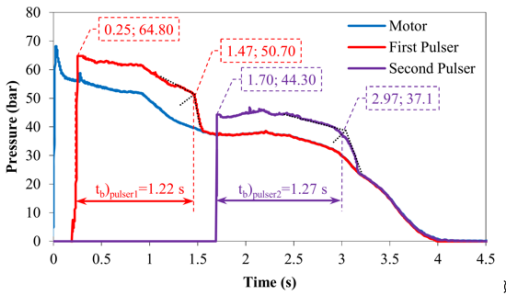

Fig. 30. Simultaneous Demonstration of Pressure Data Acquisition from Motor and Two Pulsers.

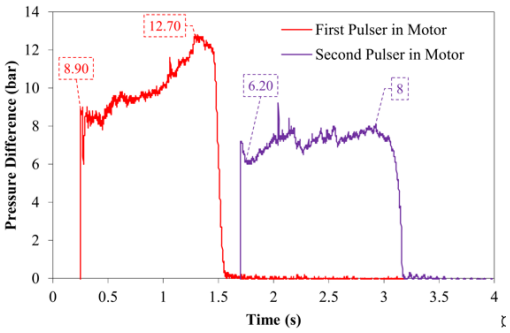

Fig. 31. Difference between Two Pulsers Pressure with Motor Pressure.

Table 2 Pulser Identification Results

Pulser	Delay Time (ms)	Action Time (s)	Pressure (bar)
Fired in ambient	51	0.625	20-30
Fired in equivalent chamber	68	0.726	30-35
Fired in motor; first	106	1.22	50-65
Fired in motor; second	46	1.27	34-45

Figure 32 represents pressure comparison of pulser test in ambient and equivalent chamber with transient analysis prediction. As shown, pressure level of pulsation in equivalent chamber is lower than pulsation in ambient and action time is vice versa. The reason is that in the first, throat diameter was 3 mm, as designed and manufactured, but in the second, throat enhanced to about 3.5 mm due to effects of the first test hot combustion products. Note that connector has been made of st-37 material. Also, decrement of the pulser test action time in ambient is due to sooner occurrence of sudden enhancement of burning surface relative to pulser test in equivalent chamber. Note that sudden enhancement of burning surface is due to faulty bonding of pulser propellant to its insulator tube. On the other hand, despite of pulser pressure prediction as neutral curve, test curves have progressive behavior due to cigarette burning nature (Sutton & Biblarz, 2010).

Solving sudden enhancement of pulser burning surface problem, adhesion processing of pulser charge to PTFE tube was revised. In addition, to avoid the problem of throat diameter, each pulser was tested in a separate position. Figure 33 represents non-dimensional comparison of pulser pressure in ambient, equivalent chamber and motor. As shown, the burning time of the pulsation in the motor have been improved to 1.22 s and 1.27 s, close to the time prediction of one second, and their curves behavior are nearly similar with no sudden enhancement.

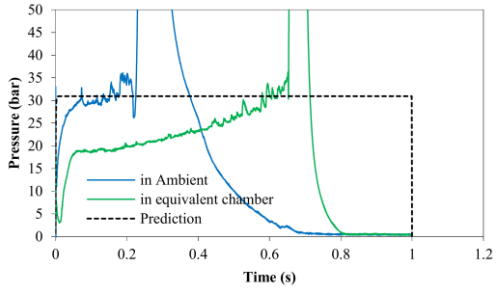

Fig. 32. Pressure Comparison of Pulser Test in Ambient and Equivalent Chamber with Prediction.

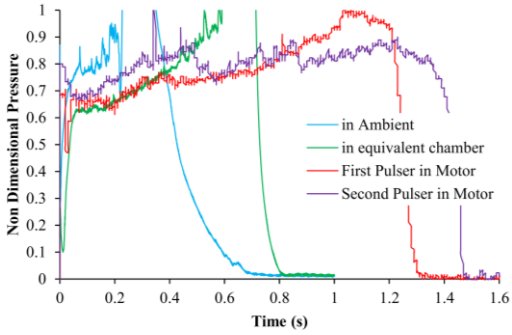

Fig. 33. Non Dimensional Comparison of Pulser Pressure in Ambient, Equivalent Chamber and Motor.

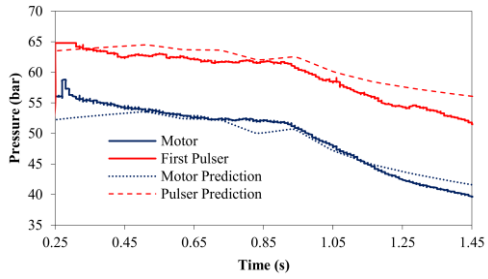

a) First Pulsation

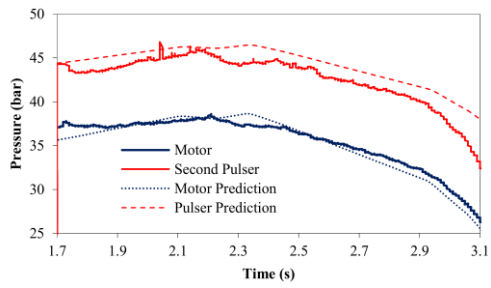

b) Second Pulsation

Fig. 34. Comparison of Motor and Pulser Pressure Test Data with Prediction.

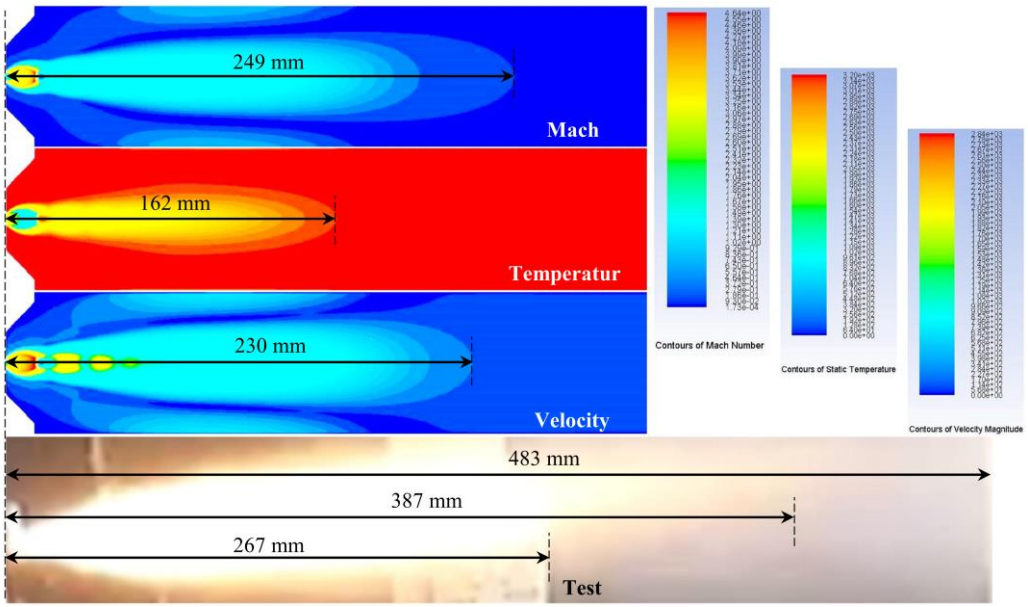

Fig. 35. Puser Plume Comparison of k − ω SST Results and Test.

As shown in Fig. 31, difference between pressures levels of two pulsers is due to motor time that pulser fires. In the first and second pulser, motor pressure varies between 40-55 bar and 30-37 bar, respectively. Figure 34 represents comparison of motor and two pulsers pressure test data with analytical prediction. As shown, pulsers pressure pattern in nearly according to performance prediction with the maximum and mean error of 16% and 4%, respectively.

Despite of using transient solution of pulser plume is better and more accurate, steady state method was used due to author's limitation on calculation space and also this is a dsirable approach used in some references. As noted later, pulser plume in ambient should have a minimum length of $L_p = 168\,mm$ due to active control design with mass flow rate of 0.015 Kg/s.

Figure 35 represents comparison of pulser plume calculation of CFD results with $\mathrm{k} - \omega$ SST model and test plume. As shown, Mach and thereafter velocity plume length in nearly close to test plume luminous core with the error of 6.7% and 13.8%. Note that CFD has solved the pulser flow field in steady state whereas test is in transient state.

6. CONCLUSION

The innovation of this research is access to a pulser with pyrogenic charge for secondary injection in a solid rocket motor. The pulsers should be designed in such a way that, in addition to providing the required flow rate for the controller, they have a suitable flame length. Design, manufacture and test of a typical pyrogenic pulser was presented and discussed. Continuity, analytical equations for transient state with viewpoint of coupling between motor and pulser chambers was wrote and solved using numerical method of fourth-order Runge-Kutta and compared with two analytical methods, resulting a good agreement. The analytic relationships governing the design of the pulser provided a suitable method for predicting the flow and length of the pulser flame. Steady state solution of pulser flow field using $k - \omega$ SST, especially in Mach contours, showed an acceptable point of view comparing with captured test plume. Comparison between analytical, CFD and test results showed that pulser pressure due to mass flow rate requirement of active control design can be estimated with a nearly good approximation. It should be considered that pyrogenic pulsers design depends on various parameters of motor and pulser charge performance prediction. The quality of pulser charge bonding to its insulator and erosion of pulser throat path due to injection play an important role to have a desirable pulser mass flow rate and plume length. The behavior of the pulser flame in the open air and the equivalent chamber and its comparison with the flame length of the flow solving was one of the interesting aspects of this project.

REFERENCES

Abdul Raheem, S. and V. Babu (2004). *Numerical Simulations of Unsteady Flows in Solid Rocket Motors.* Manchester, American Institute of Aeronautics and Astronautics.

Adams, D. M. (1967). Igniter Performance in Solid-Propellant Rocket Motors. *Journal of Spacecraft and Rockets* 4(8), 1024-1029.

Anthoine, J., Yildiz, D. and J. M. Buchlin (2000). *Nozzle Design Effect On Vortex Induced Instabilities In An Axial Injected Cold Flow Model Of The Ariane-5 EAP*. Nice, France, Institute of Noise Control Engineering, 3373-4055.

Baum, J. D. and J. N. Levine (1984). Modeling of Nonlinear Combustion Instability in Solid Propellant Rocket Motors. *Symposium (International) on Combustion* 19(1), 769-776.

Bhattacharjee, D. (2013). Experimental Studies of Active Combustion Control. *International Journal of Mechanical Engineering and Research* 3(6), 629-634.

Billoud, G., M. A. Galland, H. C. Huu and S. Candel (1992). Adaptive Active Control of Combustion Instabilities. *Combustion Science and Technology* 81, 257-283.

Blaett, L. (2011). *Vortex Driven Acoustic Flow Instability,* Tennessee: University of Tennessee, Knoxville.

Blomshield, F. S., C. A. Beiter, H. B. Mathes and J. E. Crump (1997). Nonlinear Stability Testing and Pulsing of Full Scale Tactical Motors. *Journal of Propulsion and Power* 13(3), 356-366.

Chen, Y. D. R. Guildenbechera, K. N. G. Hoffmeistera, M. A. Coopera, H. L. Stauffachera, M. S. Olivera and E. B.Washburn (2017). Study of aluminum particle combustion in solid propellant plumes using digital in-line holography and imaging pyrometry. *Combustion and Flame* 182, 225-237.

Culick, F. E. and P. Kuentzmann (2006). *Unsteady Motions in Combustion Chambers for Propulsion Systems.* California: North Atlantic Treaty Organization, California Institute of Technology.

Dehghani, M. A. (2014). *Numerical Simulation with Fluent 6.3 Software.* Tehran(Tehran): Naghoos.

Doisneau, F., A. Sibraa, J. Dupaysa, A. Murronea, F. Laurenth and M. Massoth (2012). *An efficient and accurate numerical strategy for two-way coupling in unsteady poly disperse moderately dense sprays: application to Solid Rocket Motor instabilities,* Palaiseau, France: s.n.

Ferretti, V., B. Favini, E. Cavallini, F. Serraglia and M. D. Giacinto (2011). *Pressure oscillations simulation in P80 SRM first stage VEGA launcher.* San Diego, American Institute of Aeronautics and Astronautics.

Fung, Y. T. and V. Yang (1992). Active Control of Nonlinear Pressure Oscillations in Combustion Chambers. *Journal of Propulsion and Power,* 8(6), 1282-1289.

Golafshani, M. and H. T. Loh (1989). *Computation of Two-Phase Viscous Flow in Solid Rocket Motors Using a Flux-Split Eulerian-Lag rangian Technique.* Monterey, American Institute of Aeronautics and Astronautics.

Greatrix, D. R. (2011). Scale Effects on Solid Rocket Combustion Instability Behaviour. *energies,* pp. 90-107.

Hsiao, R. C. and B. J. Saltus (2006). *A Methodology for Designing Reliable Ignition Trains in Small Ordnance Devices.* Sacramento, California, American Institute of Aeronautics and Astronautics.

Humble, R. W., G. N. Henry and W. J. Larson (1995). *Space Propulsion Analysis and Design.* Colorado: McGraw-Hill Companies.

Kostić, O. P., Z. A. Stefanović and I. A. Kostić (2015). CFD Modeling of Supersonic Airflow Generated by 2D Nozzle With and Without an Obstacle at the Exit Section. *FME Transactions* 403,107-113.

Kreyszig, E., H. Kreyszig and E. J. Norminton (2011). *Advanced Engineering Mathematics.* 10th ed. Ottawa, Ontario: John Wiley & Sons.

Luke, G. D., M. A. Eagar and H. A. Dwyer (1996). *Ignition transient model for large aspect ratio solid rocket motors.* California, American Institute of Aeronautics and Astronautics, 1-19.

Mossad, R. and R. C. Deo (2015). *Numerical Modelling of The Velocity Field of a Plane Jet Flow at Moderate Jet Exit Reynolds Numbers.* Melbourne, Australia, Csiro, p. 6.

Olaoye, O. S. and O. A. Abdulhafeez (2012). Design and Performance Characteristics of a Rocket Using Potassium Nitrate and Sucrose as Propellants. *International Journal of Science and Research* 3(8), 1892-1897.

Orieux, S., C. Rossi and D. Esteve (2002). Compact Model Based on Lumped Parameter Approach for the Prediction of Solid Propellant Micro-Rocket Performance. *Sensors and Actuators A: Physical* 101, 383-391.

Petersen, E. L. and J. W. Murdock (1990). *Active Control of Vortex-Driven Oscillations in a Solid Rocket Motor Using a Cold-Flow Simulation.* Reno, American Institute of Aeronautics and Astronautics.

Petersen, E. L. and J. W. Murdock (1999). *Control of Vortex-Induced Oscillations in a Model Solid Rocket Motor: Flow Characterization and Secondary Injection Experiments.* Los Angeles, California, American Institute of Aeronautics and Astronautics.

Poinsot, T., F. Bourienne, S. Candel, and E. Esposito (1989). Suppression of Combustion Instabilities by Active Control. *Journal of Propulsion and Power* 5(1), 14-20.

Polyanin, A. D. and A. V. Manzhirov (2007). *Handbook of Mathematics For Engineers and Scientists.*Taylor & Francis Group.

Richard, J., T. Morel and F. Nicoud (2012). Effect of the Fluid-Structure Interaction on Solid Rocket Motors Instabilities. *European Journal of Computational Mechanics* 21(3), 337-350.

Roach, R. L., K. Gramoll, M. Weaver and G. A. Flandro (1992). *Fluid-Structure Interaction of Solid Rocket Motor Inhibitors.* Nashville, American Instituteof Aeronautics and Astronautics.

Rousseau, C. W. (2011). *Establishing a Cost Effective Method to Quantity and Predict the Combustion Stability of Solid Rocket Motors Using Pulse Tests*, Matieland, South Africa: s.n.

Satyanarayana, G., C. Varun and S. Naidu (2013). CFD Analysis of Convergent-Divergent Nozzle. *Acta Technica Corviniensis*, 139-144.

Seifollahzadeh, A. and A. Aminian (2014). Simulation and Study of the Effect of Pressure Oscillations on Linear Combustion Instability in a Double Base Solid Rocket Motor. *Chemical Engineering & Process Technology* 5(2).

Sutton, G. and O. Biblarz (2010). *Rocket Propulsion Elements.* Hoboken, New Jersey: John Wiley & Sons.

Vuillot, F. (1995). Vortex-shedding phenomena in solid rocket motors. *Journal of Propulsion and Power* 11(4), 626-639.

Yang, V., A. Sinha and Y. T. Fungt (1992). State-Feedback Control of Longitudinal Combustion Instabilities. *Journal of Propulsion and Power* 8(1), 66-73.

Zhang, K. L. and S. K. Chou (2006). Performance Prediction of a Novel Solid-Propellant Microthruster. *Journal of Propulsion and Power*, January–February 22(1), 56-63.

Zhang, Q., Z. J. Wei, W. X. Su, J. W. Li and N. F. Wang (2012). Theoretical Modeling and Numerical Study for Thrust-Oscillation Characteristics in Solid Rocket Motors. *Journal of Propulsion and Power* 28(2), 312-322.

Zhao, X., Z. X. Xia, B. Liu, Z. Lv,and L. K. Ma (2018). Numerical study on solid-fuel scramjet combustor with fuel-rich hot gas. *Aerospace Science and Technology*77, 25-33.